geosciences

MDPI

Article

3D Engineering Geological Modeling to Investigate a Liquefaction Site: An Example in Alluvial Holocene Sediments in the Po Plain, Italy

Claudia Meisina [1,*], Roberta Bonì [2,*], Massimiliano Bordoni [1], Carlo Giovanni Lai [3], Francesca Bozzoni [4], Renato Maria Cosentini [5], Doriano Castaldini [6], Daniela Fontana [6], Stefano Lugli [6], Alessandro Ghinoi [6], Luca Martelli [7] and Paolo Severi [7]

1 Department of Earth and Environmental Sciences, University of Pavia, 27100 Pavia, Italy; massimiliano.bordoni@unipv.it
2 Department of Pure and Applied Sciences, University of Urbino "Carlo Bo", 61029 Urbino, Italy
3 Department of Civil and Architectural Engineering, University of Pavia, 27100 Pavia, Italy; carlo.lai@unipv.it
4 European Centre for Training and Research in Earthquake Engineering—EUCENTRE, 27100 Pavia, Italy; francesca.bozzoni@eucentre.it
5 Dipartimento di Ingegneria Strutturale, Edile e Geotecnica, Politecnico di Torino, 10129 Torino, Italy; renato.cosentini@polito.it
6 Department of Chemical and Geological Sciences, University of Modena and Reggio Emilia, 42121 Modena, Italy; doriano.castaldini@unimore.it (D.C.); daniela.fontana@unimore.it (D.F.); stefano.lugli@unimore.it (S.L.); alessandro.ghinoi@unimore.it (A.G.)
7 Geological, Seismic and Soil Survey, Emilia Romagna Region, 40127 Bologna, Italy; luca.martelli@regione.emilia-romagna.it (L.M.); paolo.severi@regione.emilia-romagna.it (P.S.)
* Correspondence: claudia.meisina@unipv.it (C.M.); roberta.boni@uniurb.it (R.B.)

check for updates

Citation: Meisina, C.; Bonì, R.; Bordoni, M.; Lai, C.G.; Bozzoni, F.; Cosentini, R.M.; Castaldini, D.; Fontana, D.; Lugli, S.; Ghinoi, A.; et al. 3D Engineering Geological Modeling to Investigate a Liquefaction Site: An Example in Alluvial Holocene Sediments in the Po Plain, Italy. *Geosciences* **2022**, *12*, 155. https://doi.org/10.3390/geosciences12040155

Academic Editors: Salvatore Grasso and Jesus Martinez-Frias

Received: 24 February 2022
Accepted: 25 March 2022
Published: 29 March 2022

Publisher's Note: MDPI stays neutral with regard to jurisdictional claims in published maps and institutional affiliations.

Abstract: Liquefaction-induced surface manifestations are the result of a complex geological–geotechnical phenomenon, driven by several controlling factors. We propose a multidisciplinary methodological approach, involving engineering geologists, geomorphologists, sedimentologists, and geotechnical engineers, to build a 3D engineering geological model for liquefaction assessment studies. The study area is Cavezzo (Po Plain, Italy), which is a municipality hit by superficial liquefaction manifestations during the Emilia seismic crisis of May–June 2012. The site is characterized by a Holocene alluvial sequence of the floodplain, fluvial channel, and crevasse splay deposits prone to liquefaction. The integration of different geotechnical investigations, such as boreholes, CPTm, CPTu, and laboratory tests, allowed us to recognize potentially liquefiable lithological units, crucial for hazard assessment studies. The resulting 3D engineering geological model reveals a strict correlation of co-seismic surface manifestations with buried silty sands and sandy silts within the shallow 10 m in fluvial channel setting, which is capped and laterally confined by clayey and silty deposits.

Keywords: liquefaction; 3D engineering geological model; Po Plain; silty sand; Holocene fluvial sequence

1. Introduction

Liquefaction has been one of the major causes of damage to structures and infrastructures in numerous early and recent earthquakes (e.g., Charleston, SC, USA, Mw 7.3, 1886; Alaska, USA, Mw 9.2, 1964; Niigata, Japan, Mw 7.6, 1964; Kobe Japan, Mw 6.8, 1995; Izmit Turkey, Mw 7.6, 1999; Christchurch New Zealand, Mw 6.3, 2011; Emilia, Italy, Mw 6.1 2012; Kaikoura New Zealand, Mw 7.8, 2016; Palu Sulawesi, Indonesia, Mw 7.5, 2018; Thessaly, Central Greece, Mw 6.3, 2021). Although the most significant liquefaction manifestations occurred in large magnitude earthquakes, conspicuous co-seismic effects, such as liquefaction, water level rise, and fractures, have also been observed in events of moderate magnitude, including the Mw 6.1 20 May 2012 Emilia earthquake in Northern Italy.

The controlling factors of the liquefaction phenomena are typically distinguished as triggering and predisposing factors. Triggering factors are related to the severity of the earthquake ground motion at a site (e.g., peak ground acceleration, duration, etc.), whereas predisposing factors are associated with the susceptibility to earthquake-induced liquefaction at a given site. This, in turn, depends on geological, geomorphological, hydrogeological (e.g., the depth of the groundwater table), and geotechnical predisposing factors. Thus, the occurrence of liquefaction at a site requires the coupled effects of both predisposing and triggering factors. Indeed, from the geological–geotechnical point of view, the liquefaction is conditioned by the depth and thickness of the potentially liquefiable layers, grain size and compaction of the sediments, and pattern of the pore water pressure re-distribution [1,2]. Previous authors performed texture and petrographic analysis to investigate the composition of sands ejected during seismic events, for a better understanding of earthquake-induced liquefaction mechanisms and to identify the possible source layers [3–5]. A thorough understanding of the non-liquefiable cap layer is also fundamental for hazard assessment [6]. Recently, Bucci et al., (2018) [7] observed that the location of the ground surface manifestation is related to the sedimentary architecture, which controls the water and sediment flow towards the surface. Therefore, accurate subsurface geological and geotechnical characterization is fundamental to identify the liquefaction-prone areas [8,9] and their potential for surface manifestations [10]. While 3D geological models have been used to address different engineering geological problems, such as land subsidence [11], gypsum dissolution [12], and urban planning [13–15], only in a very few cases [16–19] have they have been performed for liquefaction problems.

The aim of this study is to develop a new methodology for the integration of borehole logs and cone penetration tests (CPT), in order to build a 3D engineering geological model relevant for liquefaction assessment with a multidisciplinary methodological approach. The study area is the Cavezzo municipality (Italy), which was affected by liquefaction phenomena during the Emilia earthquake sequence of May–June 2012. This work was performed in the framework of the Horizon 2020 European Project "*LIQUEFACT—Assessment and mitigation of liquefaction potential across Europe: a holistic approach to protect structures/infrastructures for improved resilience to earthquake-induced liquefaction disasters*". The interested reader is encouraged to visit the website http://www.liquefact.eu/ (accessed on 21 December 2021) for more details.

The developed methodology consists of different phases. First, a lithological identification was carried out for boreholes and CPT results, and a database has been constructed, including the stratigraphic profiles from the large geological database of the Emilia Romagna Region. It contains more than 450 cone penetration tests and boreholes, in addition to laboratory analyses and new geotechnical investigations. Secondly, stratigraphic cross-sections were drawn longitudinal and transversal to the main depositional elements. The cross-sections allowed for the interpolation of the stratigraphic profiles, in order to build a 3D engineering geological model of the study area, down to the depth of 30 m. The analysis has allowed to identify the main lithological classes (sand and mud) and depositional environments (channel fill, levee, and floodplain deposits).

2. Study Area

The study area is in the Po Plain (northern Italy), on the right side of the Secchia River (Figure 1), in the Cavezzo municipality. The test site covers an area of around 27 km^2. The territory is essentially flat, with elevations gently decreasing from approximately 34 m a.s.l. in the south to approximately 16 m a.s.l. in the north. The highest topographic level runs along the Secchia River, artificial at about 7–8 m above the surrounding plain area.

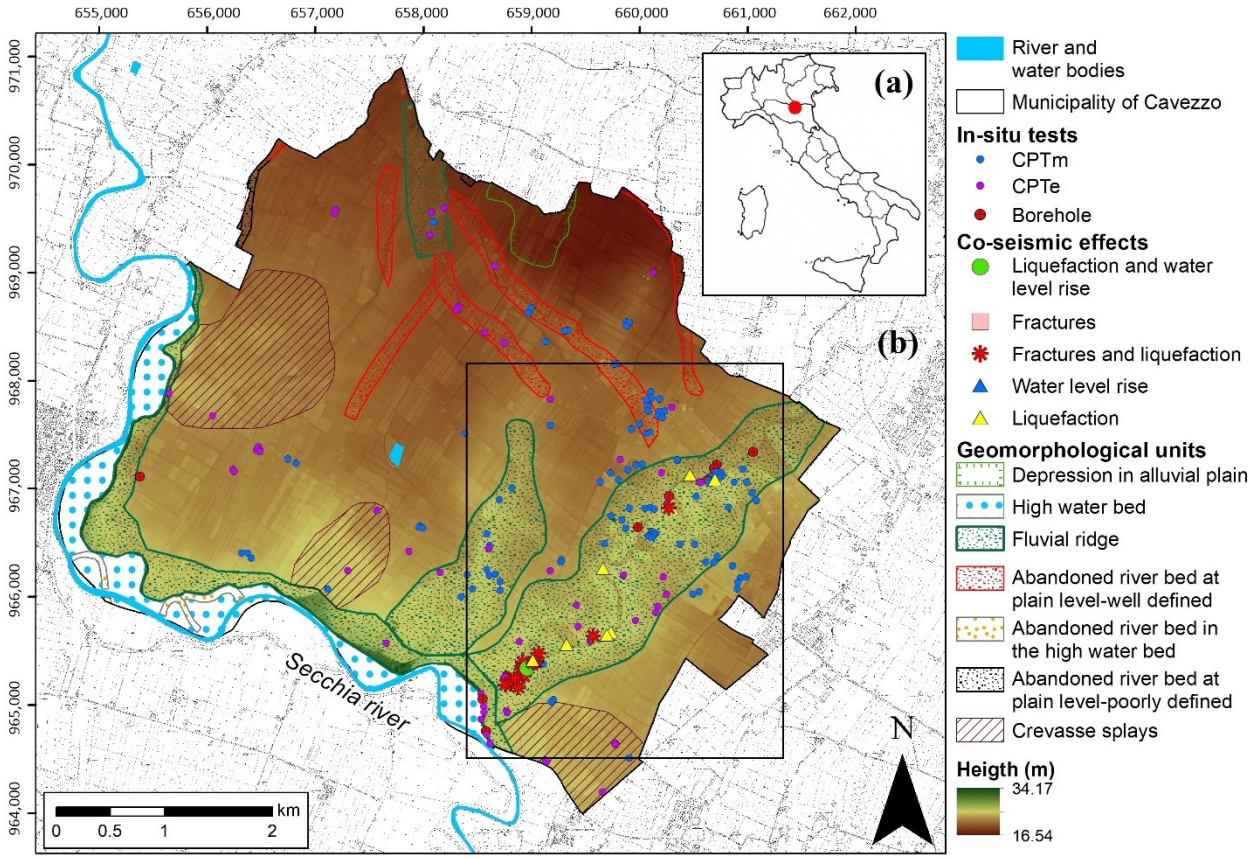

Figure 1. (**a**) Location of the Cavezzo testing site. (**b**) Geomorphological setting of the study area, digital elevation model with a spatial resolution of 1m, and distribution of the observed co-seismic effects; the available geotechnical investigations are also reported. The black box is the area of the abandoned riverbed, represented in Figure 3.

The study area is located on the southern limb of the buried Mirandola antiform [20,21]. The bedrock consists of marls and sands of the Pliocene and lower Pleistocene "Argille Azzurre" formation and middle Pleistocene "Sabbie di Imola" formation [22]. The seismic hazard of the study area is associated with the tectonic activity of the buried "Ferrara folds". The recent tectonic activity of the buried faults [23] accounts for several drainage anomalies of the alluvial plain [24]. Cavezzo is located less than 10 km far from the epicentre of the 29 May 2012 earthquake (Mw 5.8) [25]. The shallow lithostratigraphic succession was deposited mostly by the Secchia River, whereas the deeper sands from the Po River [26].

During the 29 May 2012 earthquake [27,28], co-seismic effects, such as liquefaction, water level rise, and fractures, have been observed along the buried abandoned channel of the Secchia River (Figure 1b), are located along this riverbed, which was active during Roman and Medieval times, until the 13th century.

Hydrogeological Setting

The areas most vulnerable to earthquake-induced liquefaction phenomena, according to historical information, are fully saturated, loose sandy deposits [29,30]. From the hydrogeological point of view, the subsoil of Cavezzo is mainly constituted of aquitard or aquiclude silty-clayey sequences, with layers of sand [31]. The water level of the shallow phreatic aquifer in Cavezzo is continuously monitored by three phreatimeters (Figure 2; codes MO 20-21-22), located in the first 3 m from the ground level, acquiring measurements every eight days, and managed by ARPAE Emilia Romagna (http://cloud.consorziocer.it/FaldaNET/retefalda/index, accessed on 19 December 2021).

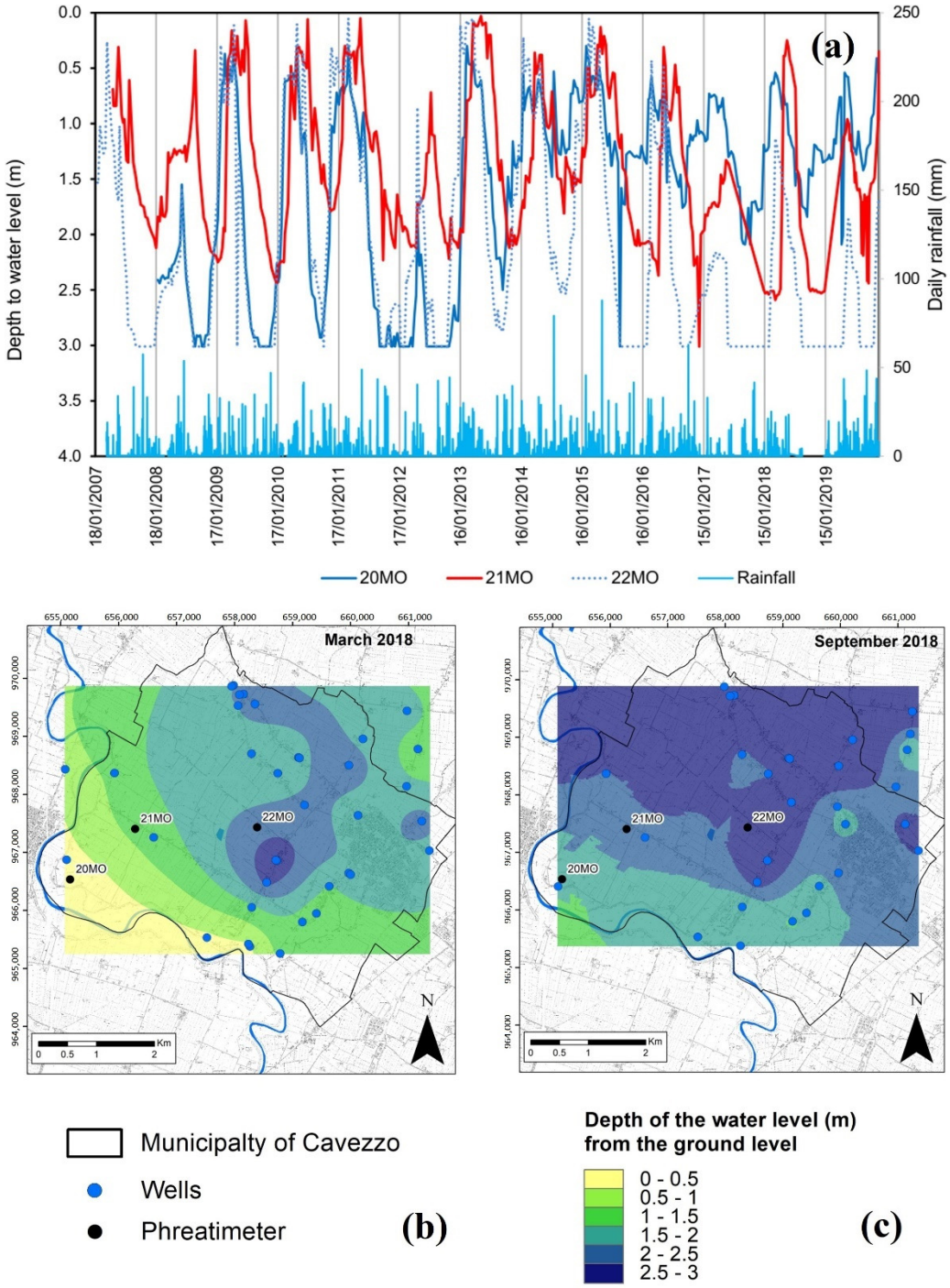

Figure 2. (**a**) Trend of the depth of the water level measured in the three phreatimeters and private wells monitored by ARPAE. The rainfall measured at Cortile Carpi (about 8 km from Cavezzo) is also shown. Depth of the water level was measured in March (**b**) and September (**c**) 2018.

The visual inspection of the phreatic level trend shows annual cyclic water level fluctuations of about 2.5 m, with a minimum in September and October and maximum in March and April (Figure 2a). These cyclic fluctuations are related to rainfall, but also to the groundwater pumping for agricultural purposes [32]. Therefore, two field campaigns were planned to measure the water level depth in private wells. Considering that the period of minimum and maximum depth corresponds to higher and lower risk for liquefaction susceptibility, these campaigns were conducted in March and September 2018, respectively. Then, the water level depth measurements (36 and 23, respectively), have been interpolated

using the Kriging approach of Geostatistics [33]. The maps of the water level depth show lower values in the proximity of the Secchia River (1 m, in March 2018) and higher values in the northern part of the study area (4–5 m deep; Figure 2). These data indicate a higher liquefaction risk in the southern part of the study area.

3. Geotechnical Investigations

For the geotechnical characterization of the site, data from previous field campaigns were collected, and new investigations were performed [34]. Overall, the data consist of borehole logs, mechanic, electric, seismic cone penetration tests (CPTm CPTu, and SCPTu), and laboratory tests, such as grain size distribution curves and Atterberg limits. In particular, the collected data belong to different databases that are listed as follows:

- Database Regione Emilia Romagna (RER);
- LIQUEFACT investigation campaigns, performed by Geostudi Astier in December 2016, as well as Geotecnica Veneta and UNIPV-DSTA (Laboratory tests) in January 2017;
- Post-2012 earthquakes geotechnical investigations (MUDE database);
- Investigation campaigns, funded by "Comune di Cavezzo" and RER, were performed by Tecnoin Geosolution and Elletipi (Laboratory tests) in December 2017 and January 2018.

3.1. Borehole and Grain-Size Distribution Analysis

We analysed boreholes 9 to 40 m deep: eight drilled along the Secchia River paleochannel, three within the artificial levee of the active riverbed, and one within the alluvial plain (Figure 1).

Figure 3 shows the location of the sampled sand boils and boreholes, analysed by the engineering and geotechnical laboratories of the University of Pavia and Modena. Additional information is provided in Table S1, in the Supplementary Materials.

The grain-size analysis identified the following lithological classes (LC): clay (A), clay with peat (At), clayey silt (La) clayey sandy silt (Las), silty sand (Sl), sandy silt (Ls), and sand (S).

In the shallow sequence, from 0 to 10 m from the ground level, two main lithological populations were recognized: (i.) clayey silt (La) and clayey sandy silt (Las) (Figure 4); (ii.) silty sand (Sl), sand (S), and sandy silt (Ls) (Figure 5); in the sequence deeper than 10 m, the sediments were (iii.) clayey silt (La) and clay (A) (Figure 6).

Grain-size analyses of sand boils, ejected near the borehole 16-138-S1 (Uccivello sand boil, see the location in Figure 3), were compared with the sand from the subsurface (Figure 5).

3.2. Cone Penetration Tests

The mechanical and electrical cone penetration test (CPTm and CPTu) results were used to draw the stratigraphic logs to build the 3D engineering geological model. The CPTu provides pore water pressure (u) values, sampled every 2 cm, whereas the CPTm is sampled every 20 cm.

Thus, the mechanical and electrical cone penetration test interpretation is performed using the classifications of Robertson (1990) [35] and Schmertmann (1978) [36] for CPTu and CPTm, respectively.

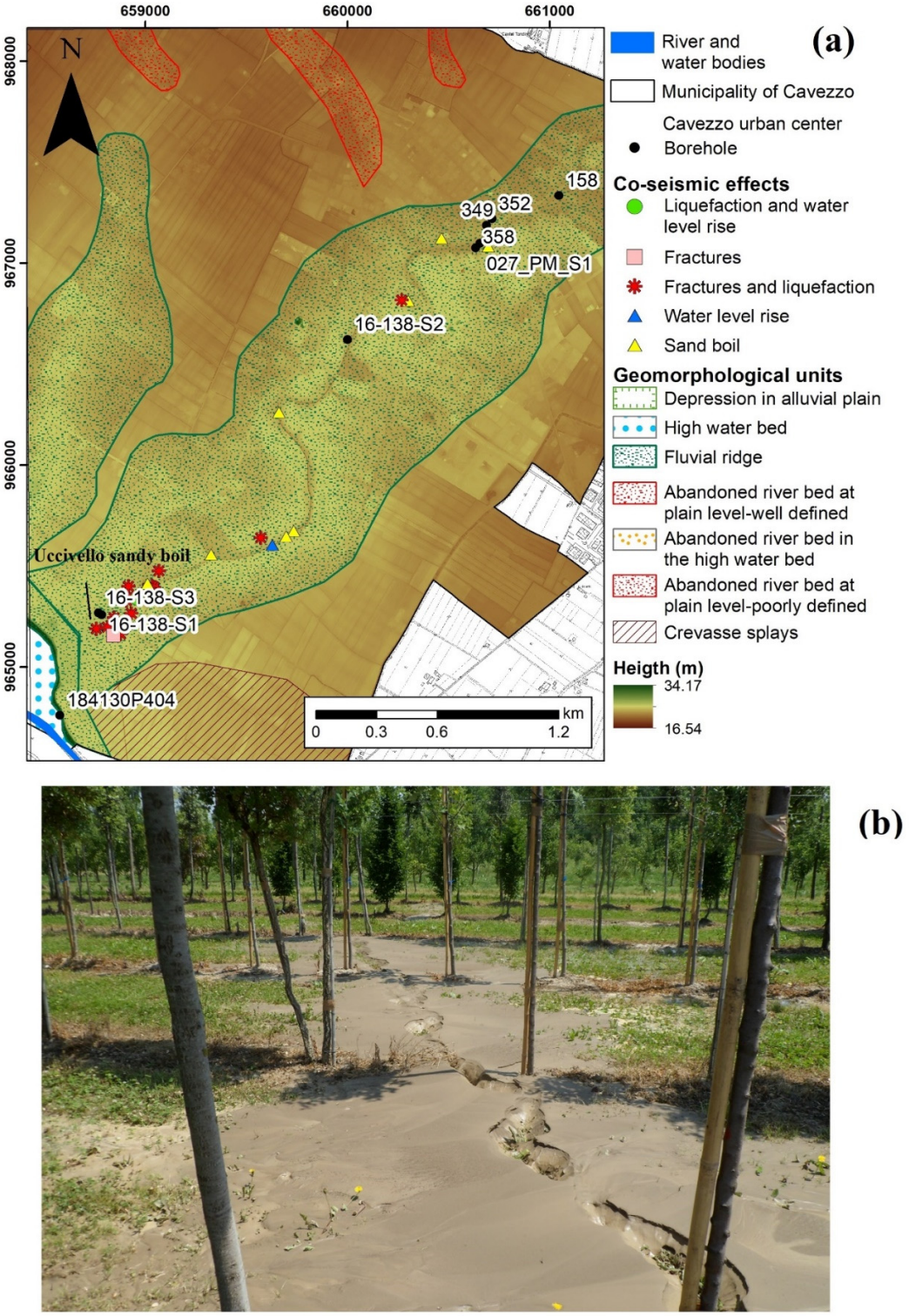

Figure 3. (**a**) Location of the boreholes sampled for classification tests; (**b**) Uccivello sand boil.

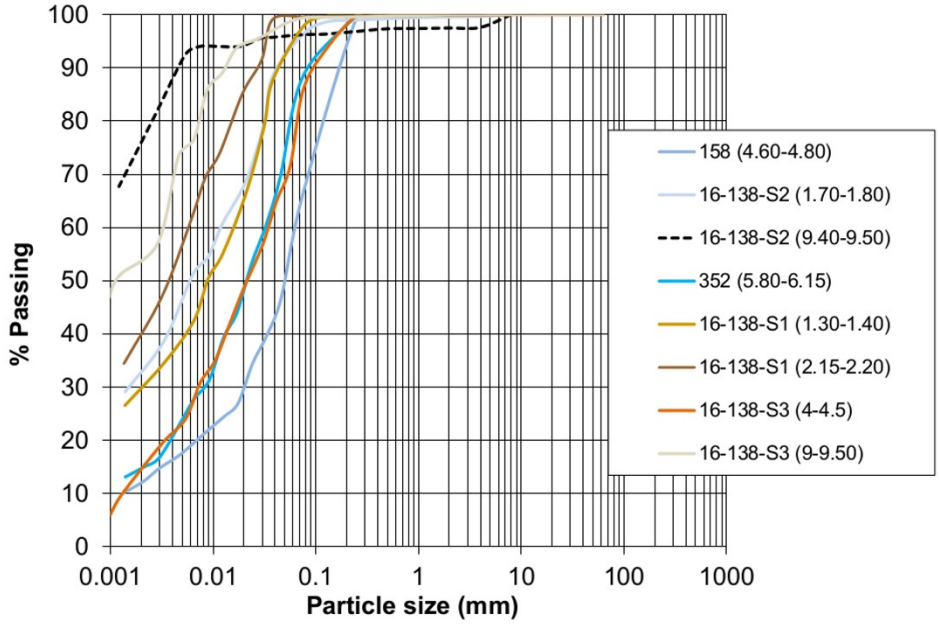

Figure 4. Particle size distribution curves for the clayey silt (La) and clayey sandy silt (Las) in the shallow 10 m from the ground level. The dotted black curve refers to a sample rich in organic matter.

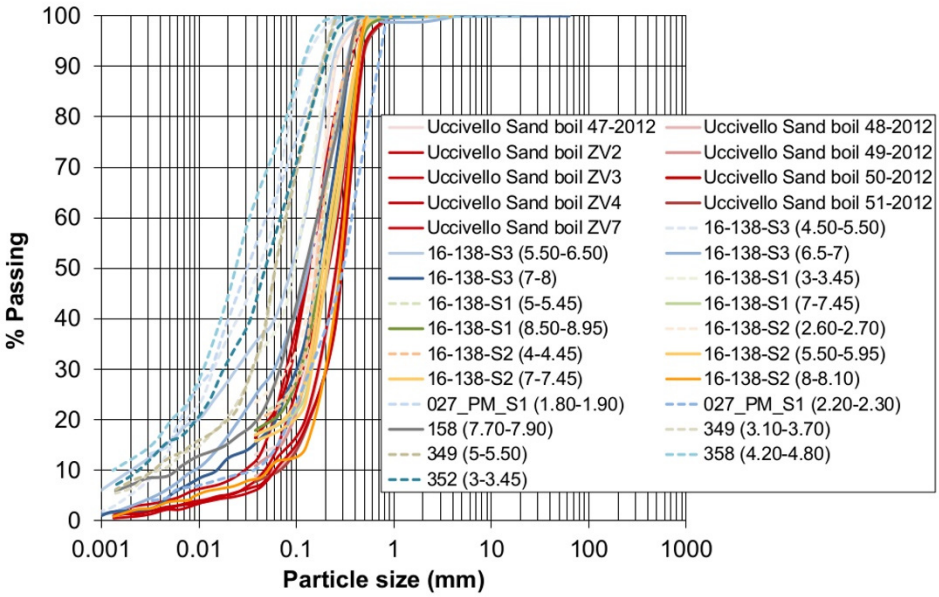

Figure 5. Particle size distribution curves for silty sand (Sl), sand (S), and sandy silt (Ls).

The chart of Robertson (1990) [35] allows for distinguishing nine soil types (normalized soil behaviour type, SBTn classes). The radius of concentric circles of the chart can be used as soil behaviour type index, Ic. The Schmertmann (1978) [36] approach allows us to classify of different lithotypes. Geologismiky Geotechnical, CPeT-IT v 1.6, and GeoStru-Static Probing software were used to analyse the CPTu and CPTm measurements, respectively.

A correspondence table (Table 1), among the lithotypes of the Schmertmann (1978) [36] classification and Robertson (1990) SBTn classes [37], was implemented to harmonize the CPT results with the stratigraphic logs of the boreholes [37].

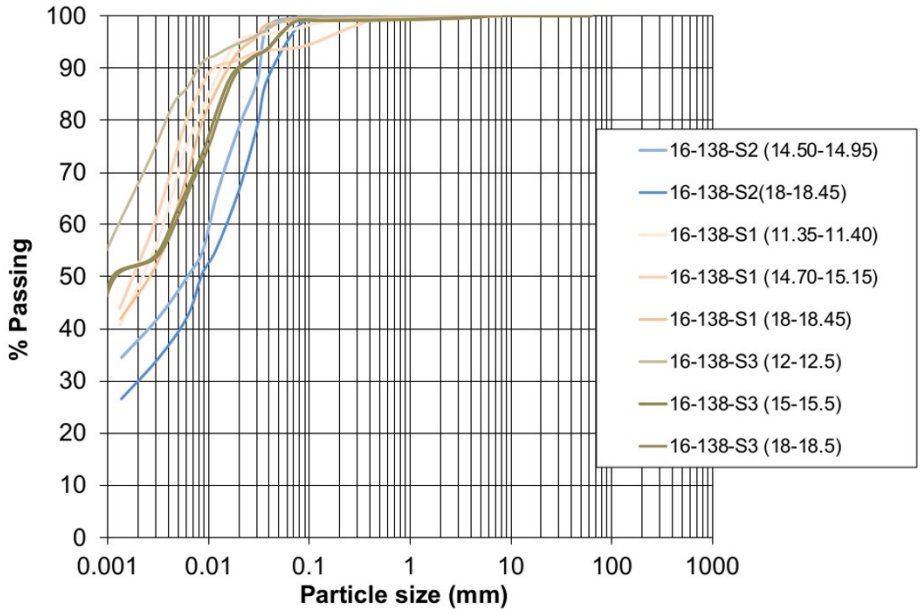

Figure 6. Particle size distribution curves for clayey silt (La) and clay (A) deeper than 10 m.

Table 1. Correspondence among the soil classification from Schmertmann (1978) [36] and SBTn from Robertson (1990) [37] and the lithological classes (LC) detected using the borehole logs.

LC from Boreholes	Soil Classification from Schmertmann (1978) [36]	Ic Range	SBTn from Robertson (1990) [37]
Clay with peat (At)	Organic clay and mixed soils	Non-liquefiable clay with peat soils Ic > 3.5	2
Clay (A) and clayey silt (La)	Insensitive non fissured inorganic clays	Non-liquefiable silt/clayey soils 2.6 < Ic ≤ 3.5	3–4
Sandy silt (Ls) and clayey sandy silt (Las)	Sandy and silty clays clayey sands and silts	Sandy silts and non-plastic silts 2.1 < Ic ≤ 2.6	5
Sandy silt (Ls) and silty sand (Sl)	Silt–sand mixtures	Sands with small amount of fines 1.8 < Ic ≤ 2.1	6
Sand (S)	Sands	Clean sands 1.3 < Ic ≤ 1.8	7

Among the seven dominant lithologies, the clayey silt (La) was included with the lithological class of the clay (A), being not liquefiable soils, and the lithological class of the clayey sandy silt (Las) was included in the sandy silt (Ls).

The anthropogenic deposits were distinguished using the boreholes and cone penetration tests. The thickness of these deposits was estimated, considering the depth interval with qc and fs is higher than the other values measured along with the entire profile, representing anomalous measurements. An example is reported in Figure 7.

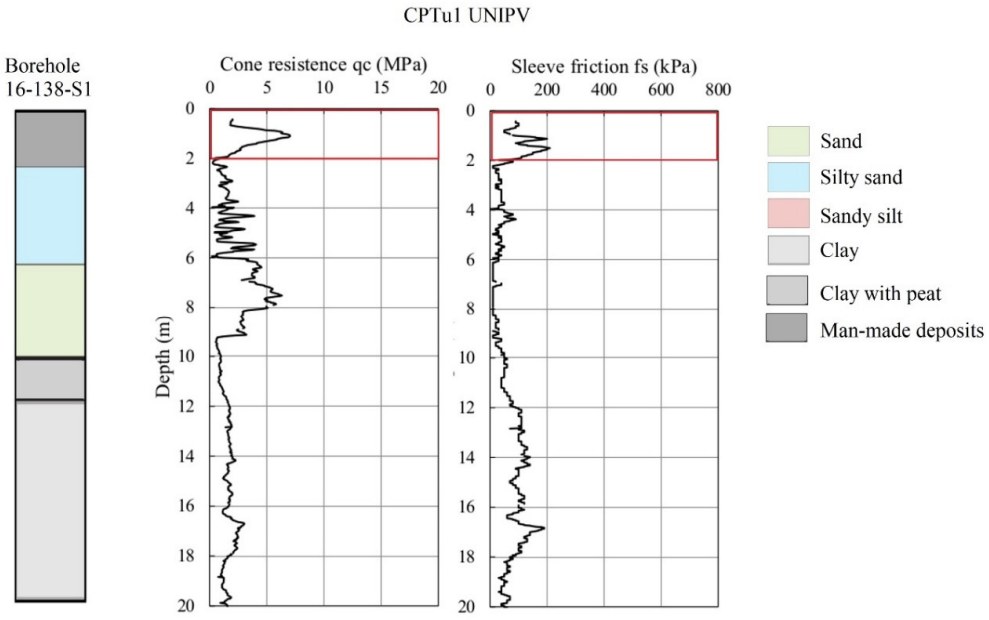

Figure 7. Comparison of a pair of boreholes and CPTu measurements (qc and fs), including the detection of the thickness of the anthropogenic deposits (red box).

4. Methodology

The developed methodological approach is aimed to reconstruct the 3D engineering geological model, in order to identify the sandy layers susceptible to liquefaction phenomena, using boreholes, cone penetration tests, and classification tests (Figure 8). The outputs of the 3D engineering geological model are used as the starting point to analyse the subsurface architecture, in order to distinguish homogeneous areas for liquefaction hazard assessment. The solid modeling approach has been adopted to construct the 3D engineering geological modelling architecture of Cavezzo [38].

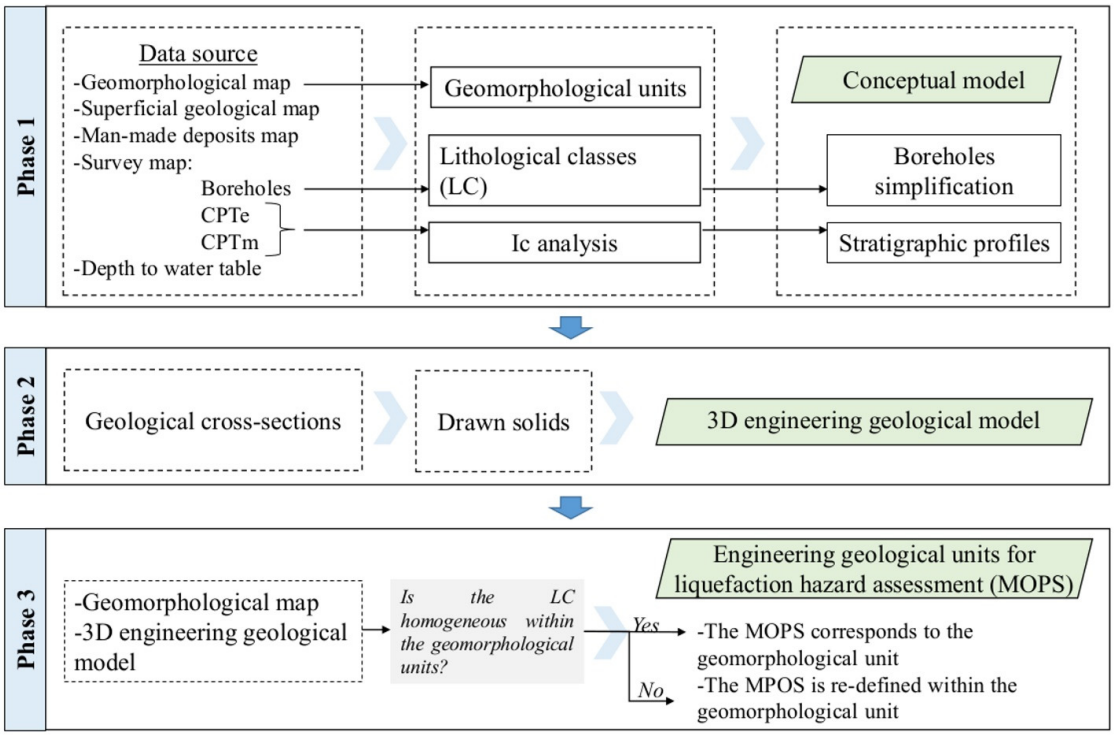

Figure 8. Flow-chart of the methodological approach.

The software used to develop the geological model is Groundwater Modelling System (GMS) Aquaveo. The methodology consists of three phases, described as follows:

- Phase 1. Conceptual model The first phase is aimed to collect and harmonize the data. The stratigraphic profiles of the 30 m deep sequence, obtained using boreholes logs, mechanical, and electrical cone piezometric tests, are compiled using the detected lithological classes. The database includes the geographic coordinates of each stratigraphic profile, as well as the depth and thickness of each layer.
- Phase 2. 3D engineering geological modelling In the second phase, geological cross-sections are manually drawn by correlating the different lithological units to generate the 3D engineering geological model [39]. The geological cross-sections are drawn longitudinal and transversal to the depositional elements and focus on areas characterized by significant vertical and horizontal variations. The engineering geological model is built up using the "horizons to solids" algorithm via the Groundwater Modelling System (GMS) Aquaveo software. The horizons are numbered consecutively from the bottom to the top. A primary TIN (triangulated irregular network) is created to obtain the 2D mesh of the surface, defining the spatial resolution of the model. The cross-sections are used as a guide, and the horizons allow us to interpolate a surface for each layer.
- Phase 3. Engineering geological units for liquefaction hazard assessment (MOPS) The third phase is aimed to delineate the engineering geological units or microzone for seismic liquefaction hazard assessment (MOPS; "Microzone Omogenee in Prospettiva Sismica" *sensu stricto* [40]). The MOPS are homogeneous areas, showing similar trends in the depth of Ic behavioural parameters and described by a representative stratigraphic profile.

5. Results

5.1. Conceptual Model

All available geotechnical investigations, including the boreholes and cone penetration tests, were exploited to determine the soil stratigraphy and identify the soil type. The stratigraphic profiles were used to build the architecture of the subsoil model of the top 30 m sequence. For the borehole log interpretation, layers thinner than 40 cm were included in the lithological classes, located at the top or bottom, with similar soil behaviour type values. Therefore, the resulting vertical resolution of the model is approximately 40 cm. The analysis of cone penetration test, performed in a 20 m zone from the boreholes, confirms that these deposits have soil behaviour type index values comparable with the sandy silt (Ls).

The comparisons between pairs of boreholes and cone penetration tests within a distance of 20 m give insight into the difference in the stratigraphic profiles obtained using boreholes and cone penetration tests. Indeed, as previously reported, the sandy mixtures are not well-identifiable [41,42]. In some cases, the sandy silt and silty sand layer, detected using boreholes, are classified as clayey soils (Figure 9).

For this reason, a correction of the Ic was applied to increase the reliability of the CPTu and improve the stratigraphic profiles obtained by these different geotechnical investigations.

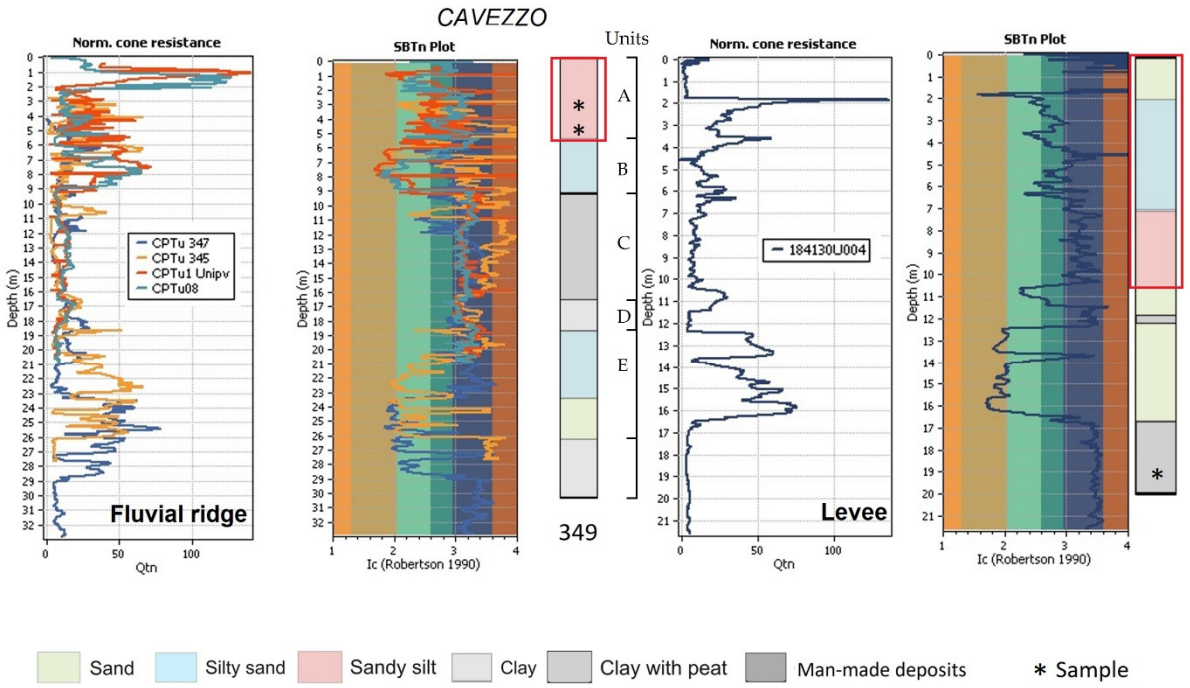

Figure 9. Comparison of normalized cone resistance (Qtn) and Ic versus the representative stratigraphic logs of the borehole for two depositional units, such as fluvial ridge and levee. The red box represents the sandy layers not recognized using the cone penetration tests.

Even though numerous subsurface investigations previously carried out in Cavezzo for urban planning purposes and post-earthquake reconstruction, no comprehensive studies to harmonize and interpret the results are available. In this work, the 3D engineering geological model was constructed by laboratory and in situ tests. Overall, the lithostratigraphic architecture of the top 30 m of the sequence shows that the study area is characterised by significant vertical and horizontal variations. The resulting simplified conceptual model has been used to interpret the engineering properties of soils. In particular, five stratigraphic units were identified (Figure 10):

- Unit A; heterogeneous deposits, lithological classes clayey silt, and clayey sandy silt (La, Las), with interbedded thin silty sand (Sl) layers, corresponding to the recent alluvial plain;
- Unit B; lithological classes sand (S), silty sand (Sl), and sandy silt (Ls), corresponding to the fluvial channel, and these deposits are the source of most of the visible liquefaction effects;
- Unit C; clay (A) and clay with peat (At), corresponding to the palustrine depositional environment;
- Unit D; clay (A) of the ancient alluvial plain;
- Unit E; dense sands of the ancient fluvial channel.

In the area of the NE–SW fluvial ridge in the urban zone of Cavezzo (Figure 1), the analysis of the cone resistance (qc) and sleeve friction (fs) shows a high lateral and vertical lithological variability, due to the facies transition between channel and levee. The values of qc are not uniform for the shallow 5–10 m from the ground level, moving from the northern and southern portion of the fluvial ridge, made up of sandy layers, ranging from 1.5 to 5 MPa. From 15 to 20 m below the ground level, the qc values of the deeper sands are higher, ranging from 2 to 15 MPa.

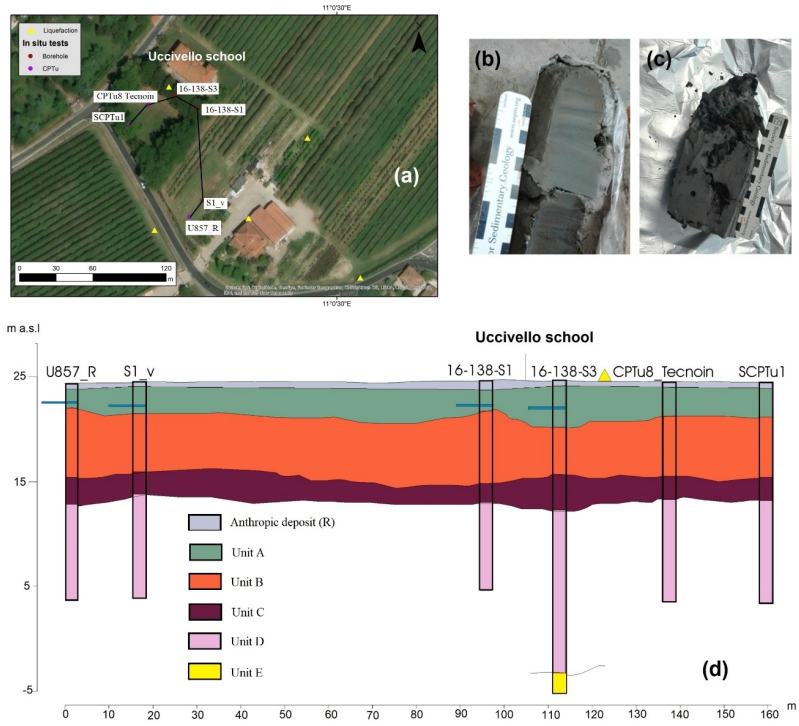

Figure 10. (**a**) Location of the geological cross-section (black line) near Uccivello school (about 2 km SW of Cavezzo urban center). (**b**,**c**) Sample from the borehole 16-138-S3 at depths of 5.50–6.5 and 10.85–11.50 m, showing the shallow sequence of thin levee layers and organic matter-rich clayey soils, respectively. (**d**) Simplified geological cross-section near Uccivello school. The liquefaction phenomena (yellow triangles) and groundwater level (blue lines) are also reported.

In the abandoned riverbed at the plain level (Figure 1), shallow sandy layers show qc values similar to the fluvial ridge. The thickness of these sediments is lower than that of the sandy soils localized in the fluvial ridge. Few cone penetration tests are available to analyse the lithological variabilities of the crevasse splays. These geomorphological contexts display interbedded thin layers of sandy silt and silty sand, with qc values not very different, with respect to the values measured in the fluvial ridge and abandoned riverbed at the plain level. In the alluvial plain, sandy layers are present in the first two meters from the ground level, with values of qc ranging from 0.6 to 4 MPa.

5.2. Construction of a 3D Engineering Geological Model

The 3D engineering geological model of Cavezzo was constructed with a spatial resolution of 20 m, using 10 borehole logs and 164 stratigraphic profiles, obtained using 111 mechanical cone penetration, 32 electrical cone penetration, and 21 seismic cone penetration tests (Figure 1). The resulting model shows 24 horizons (Figure 11a). The first one is represented by the anthropogenic deposits, distributed over the entire area, reaching a maximum thickness of 2 m in the urban area. The 3D north-to-south and west-to-east cross-sections (Figure 11b) show a higher heterogeneity in the fluvial ridge, with lenses of sandy silt and silty sand, whereas continuous horizons are present in the floodplain. In the southern sector of the fluvial ridge, where liquefaction phenomena were observed (Figures 1 and 3), four main stratigraphic units are present (Figure 11c). Underneath the anthropogenic deposits, a superficial clayey silt and sandy silt layer, 2 to 4 m-thick, with a low percentage of sand (from 2 up to 13%), is present. The layer below is constituted by sand, sandy silt, and silty sand, with a thickness of 5–7 m. The sand content of these deposits ranges from 50 to 80%, as reported in Section 3.1. The third stratigraphic unit is characterised by clay with peat and clay. In the deepest unit, clayey deposits are present.

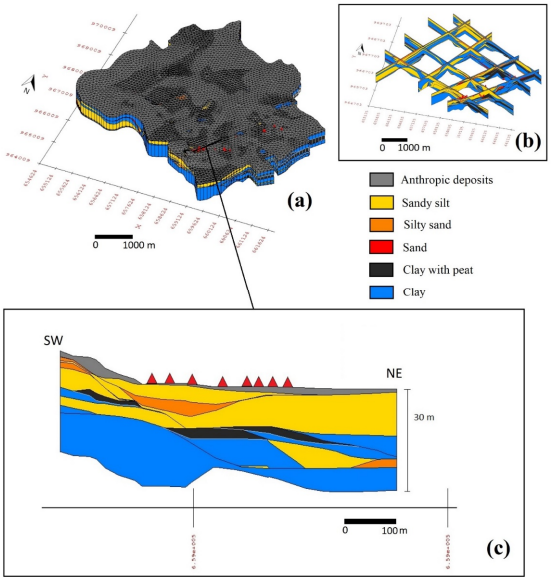

Figure 11. (**a**) The 3D engineering geological model of Cavezzo and fence diagram of geological sections, derived from the model showing the lithological variations. (**b**) Detail of a cross-section through the observed sand boils. (**c**) Liquefaction phenomena are represented as red triangles.

Overall, the model displays a superficial coverage of sandy silt, with a higher content of fine with a thickness, ranging from 2 to 15 m. The higher thickness of these shallow deposits is observed in the floodplain. Below these deposits, sandy layers are present. These deposits are not laterally extended and mainly localized in the fluvial ridges and abandoned riverbeds at the plain level. The thickness of these soils ranges from about 4 to 6 m. The deeper deposits are constituted by clay and clay with peat, with the last one representing a marker layer, useful for the stratigraphic correlations.

Over 15–20 m from the ground level, fine sandy soils are present, corresponding to the ancient fluvial channel deposits.

Furthermore, the reliability of the 3D modelling has been assessed by performing a statistical analysis of the spatial distribution of the geotechnical investigations. The kernel density analysis has been implemented to estimate the density of the geotechnical investigations in a neighborhood around these points [43]. A total of 33% of the study area is characterized by values from moderate to high density, and it is evident that the density of the data used to create the 3D engineering geological model is higher where the liquefaction phenomena were observed, and the geological setting is more complex, due to the deposits of the buried paleochannel of the Secchia River (Figure 12).

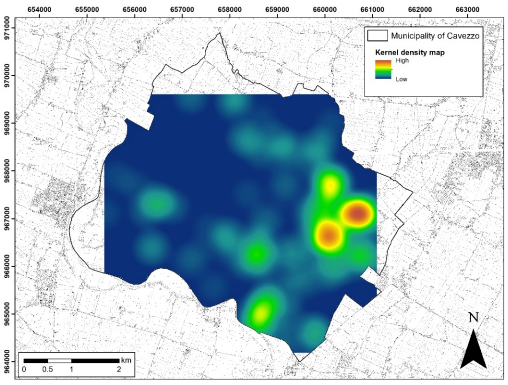

Figure 12. Kernel density map of the geotechnical investigation used to create the 3D engineering geological model of Cavezzo. The extension of the map is limited to the distribution of the available points.

5.3. Engineering Geological Units for Liquefaction Hazard Assessment (MOPS)

The analysis shows that the study area is characterized by nine MOPS. The liquefiable layers were identified in all the MOPS, except for MOPS 9, corresponding to the alluvial plain sector (Table 2). These liquefiable soils include sandy silts or silty sands, as well as sands mainly localized in the shallow 2–15 m from the ground level. Although the liquefiable layers are evident in all the MOPS, field evidence and observed co-seismic effects, after the 2012 earthquake, indicate that only MOPS 5, 6, and 7 were affected by liquefaction (Figure 13). In MOPS 5 and 7, silty sands and sandy silts are located between 2 and 12 m from ground level, in most cases capped by a clayey soil of about 1 m thick. Clayey deposits are not superimposed on the liquefiable deposits (such as silty sands and sandy silts), in correspondence with the MOPS 6. Even if surface manifestations of liquefaction can be evident in areas with no low permeability cap present, the 3D engineering geological model of Cavezzo displays that, in this case, the field evidence of liquefaction are observed in correspondence of silty sands and sandy silts layers in MOPS 5, 6, and 7, which are confined by clayey and silty deposits, both vertically and laterally, forming bodies that were extended not more than a few hundreds of meters in the lateral direction. These results agree with previous findings for the co-seismic liquefaction phenomenon observed in other sites in Emilia Romagna [27,44–47]. The sandy silts and silty sands layers, identified in the other MOPS, where no liquefaction phenomena were detected, are continuous bodies not confined by clayey-silty deposits.

Table 2. Lithological and geomorphological characteristics of the MOPS in Cavezzo.

MOPS	Description	Depositional Environment	Depth of the Water Level (m) from Ground Level (March 2018)
1	Liquefiable sandy silt layers, between 2 and 9 m from ground level.	Abandoned riverbed	1.5–2.0
2	Liquefiable sandy silt layers, between 2 and 12 m from ground level.	Abandoned riverbed and ancient fluvial ridge	1.0–3.0
3	Liquefiable sandy silt layers, between 3 and 6 m from ground level.	Crevasse splay	2.0–2.5
4	Liquefiable sandy silt layers, between 2 and 9 m from ground level.	Crevasse splay	2.0–2.5
5	Liquefiable sandy silt and silty sand layers, between 2–9 and 9–12 m from ground level, respectively.	Abandoned river bed and ancient fluvial ridge	1.5–2.0
6	Liquefiable sandy silt and silty sand layers, between 2 and 8–9 m from ground level.	Abandoned river bed and ancient fluvial ridge	1.0–1.5
7	Liquefiable sandy silt and silty sand layers, between 2–9 m and 9–15 m from ground level, respectively.	Abandoned river bed and ancient fluvial ridge	1.0–1.5
8	Liquefiable sandy silt layers, between 9 and 14 m from ground level.	Levees and actual riverbed	1.0–1.5
9	Non-liquefiable silt/clayey soils.	Alluvial plain	1.0–5

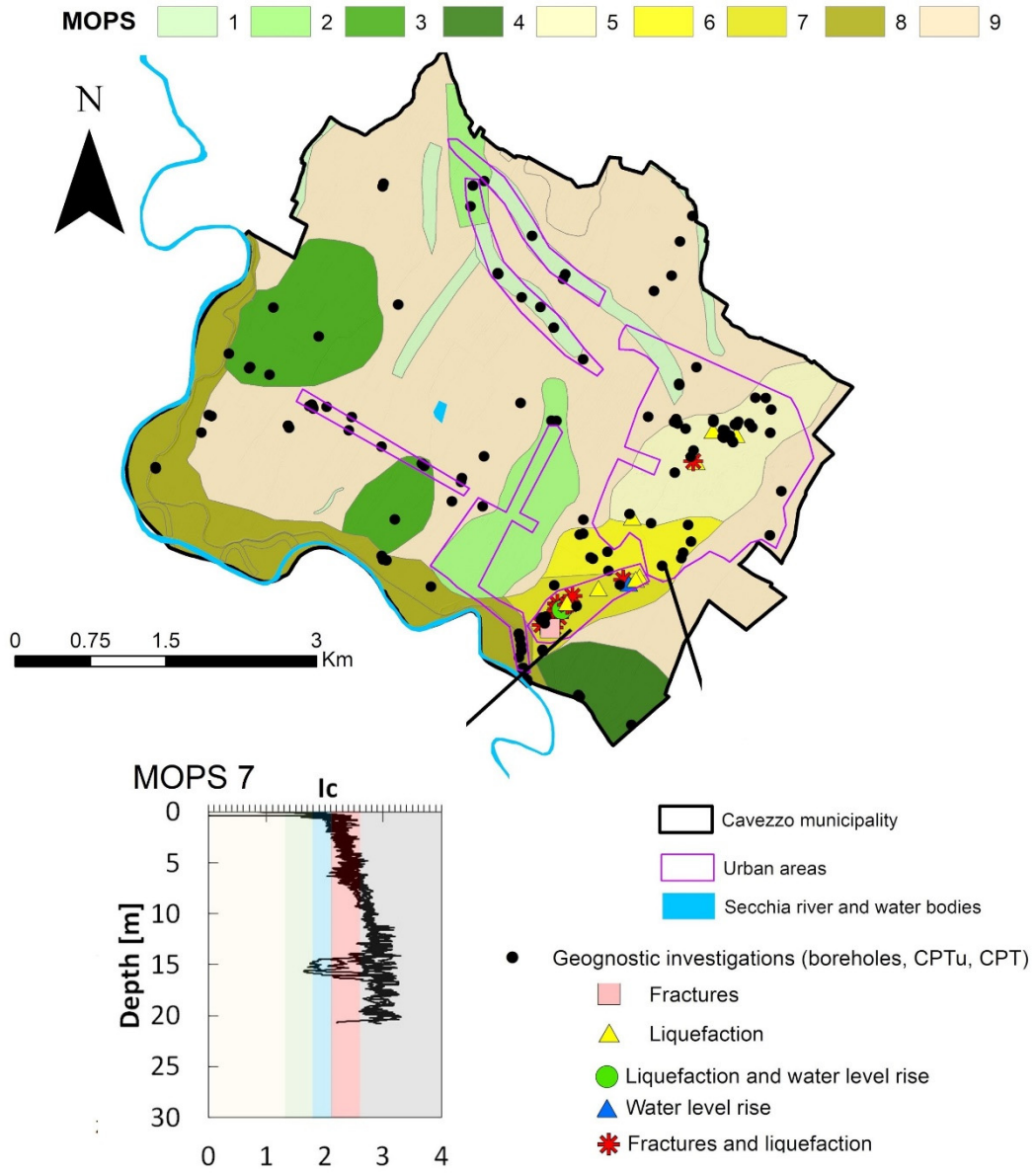

Figure 13. Lithological units (MOPS) in Cavezzo. The Ic trend for MOPS 7 is also reported.

6. Discussion

In this section, the contribution of the 3D engineering geological model for liquefaction studies is discussed. In particular, the 3D engineering geological model, reconstructed for Cavezzo, was used to support the identification of the liquefaction source layer and mechanisms that may control the ejection to the surface.

6.1. Influence of the Sedimentary Architecture on the Surface Manifestations of Liquefaction

Previous authors observed that the surface manifestations of earthquake-induced liquefaction occur when a base layer of liquefiable soils is overlaid by a confining layer, known as the cap or crust [6,47,48]. In particular, Ishihara (1985) [6] introduced an empirical approach, based on the relationship between the thickness of the liquefiable layer and the thickness of the overlapping non-liquefiable layer, to assess the potential for ground manifestation of liquefaction. The author analysed the liquefaction observed after three large earthquakes occurred in China and Japan, with Mw > 7.5. In this Section, the 3D engineering geological model of Cavezzo was exploited to extract the thickness of the liquefiable and non-liquefiable layer, in order to understand the mechanisms that may

have controlled the surface manifestations of liquefaction. The superficial sandy silt, with a very low content of sand, is considered as the potential non-liquefiable layer, and the underneath silty sand is identified as the liquefiable layer. A grid of 20 m was created, and a centroid was carried out for each cell of the study area. For each point, the values of the thickness of the non-liquefiable (H1) and liquefiable (H2) layers were assigned. Layer thickness data were plotted in the graph of Ishihara (1985), also reporting the points of different types of observed co-seismic effects (Figure 14). Most of the observed liquefaction and water level rise, as well as the fractures and liquefaction phenomena, are correctly predicted by the bounds introduced by Ishihara (1985), except for some liquefaction sites. These misclassified points could be due to the presence of laterally drifted conduits of the sand boils in the area with higher thickness of the liquefiable soils (Youd and Garris, 1995). The results are consistent for the area of the Uccivello sand boils localized in the southern zone of the fluvial ridge, aligned along the NE-SW direction. Therefore, the ground surface manifestations observed in the studied area seem to be related to sandy layers of about 1–3 m thick in the upper 10 m from the ground level, laterally and vertically confined.

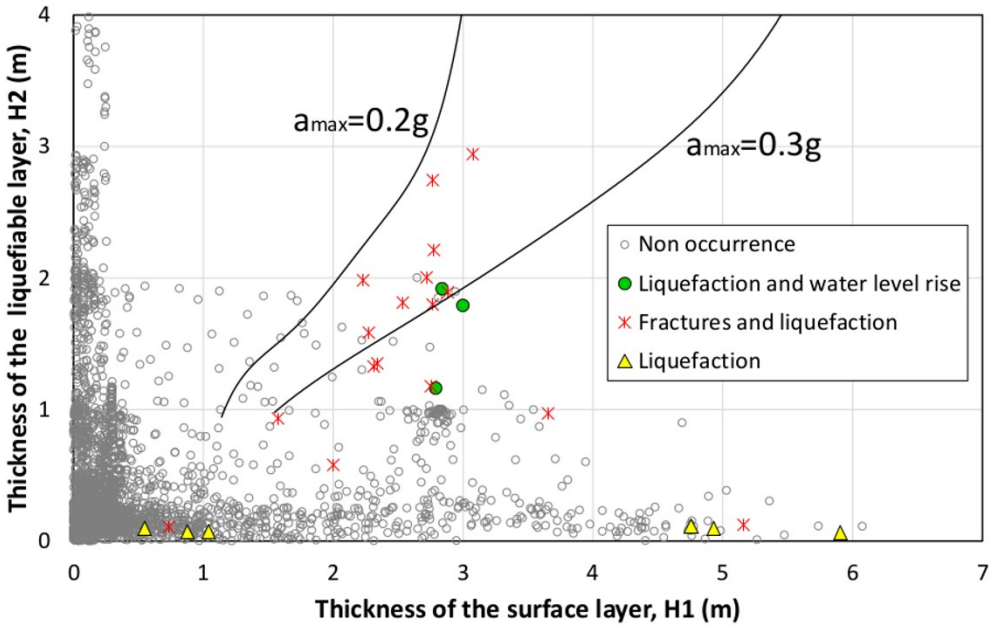

Figure 14. The thickness of liquefiable (H2) versus the thickness of the non-liquefiable (H1) layers for Cavezzo distinguishing the non-occurrence points and ground surface manifestations of liquefaction. The bounds introduced by Ishihara (1985) [6] are also reported.

6.2. Composition of the Liquefied Layers

The examined sands from boreholes and sand boils have an overall lithoarenitic composition, distinctive of the Secchia River [49]. The lithic association includes sedimentary fine-grained siliciclastic grains (siltstones and shales) and carbonate lithics (largely micritic limestones and calcite spars). Shales are well-lithified and -rounded, with an evident iso-orientation of the clay minerals; for these characteristics, they appear to have a detrital origin, derived from the erosion of the pelitic successions cropping out in the Northern Apennines. The comparison of the composition of the sand boil sand with the buried sands indicates a close similarity with the shallow sands, down to the depth of 4.5 m. These shallow sands are discriminated from the deeper ones, which are richer in carbonate grain content.

7. Conclusions

The paper proposes an innovative multidisciplinary approach to understand the earthquake-induced liquefaction manifestations at the ground surface by constructing a 3D

detailed engineering geological model. The proposed methodology allows us to facilitate the joint use of different direct and indirect surveys, such as boreholes, CPTm, and CPTu. The methodology allows to detect potentially liquefiable engineering geological units, essential for hazard assessment (MOPS), using the spatial variation of the behavioural index Ic, obtained from the interpretation of CPTm and CPTu test results. Indeed, the methodology allows us to identify the liquefiable layers and their geometry in a complex geomorphological and lithotechnical context, located in an alluvial plain, characterized by fluvial depositional bodies prone to liquefaction. Confined sandy silts and silty sands bodies, susceptible to liquefaction, were recognized, especially in areas where the depth of the water level is shallower. The 3D engineering geological model highlights the subsoil architecture of these bodies in the subsoil, which matches with the surface manifestations of liquefaction that were observed after the seismic sequence in 2012.

The results show that the depositional geometry should be considered to identify the prone areas to co-seismic surface manifestations. These results may be significant for the study of liquefaction in other similar contexts.

Supplementary Materials: The following are available online at https://www.mdpi.com/article/10.3390/geosciences12040155/s1, Table S1. Summary of the information about the samples, extracted from boreholes in Cavezzo. LC stands for lithological class. FC stands for fine content.

Author Contributions: Conceptualization, C.M., R.B., C.G.L. and F.B.; methodology, C.M. and R.B.; software, R.B.; validation, all the authors; investigation, all the authors; data curation, M.B., R.M.C., D.C., D.F., S.L., A.G., L.M. and P.S.; writing—original draft preparation, R.B.; writing—review and editing, all the authors.; supervision, C.M. and C.G.L.; funding acquisition, C.G.L. All authors have read and agreed to the published version of the manuscript.

Funding: This research has been carried out within the framework of the European LIQUEFACT project. The LIQUEFACT project has received funding from the European Union's Horizon 2020 Research and Innovation Programme, under grant agreement no. 700748.

Data Availability Statement: All data generated or analysed during this study are included in this article, and the datasets used or analysed during the current study are available from the corresponding author on reasonable request.

Acknowledgments: This research has been performed in the framework of the European LIQUEFACT project. The LIQUEFACT project has received funding from the European Union's Horizon 2020 Research and Innovation Programme, under grant agreement no. 700748. This support is gratefully acknowledged by the authors. A word of gratitude is also expressed by the University of Pavia and Eucentre to the administration of Cavezzo Municipality for their support in the microzonation of this town. The authors are grateful for the support of the work performed by G. Cerra and G. Perotti, in the framework of their master thesis.

Conflicts of Interest: The authors declare no conflict of interest.

References

1. Albano, M.; Barba, S.; Solaro, G.; Pepe, A.; Bignami, C.; Moro, M.; Saroli, M.; Stramondo, S. Aftershocks, groundwater changes and postseismic ground displacements related to pore pressure gradients: Insights from the 2012 Emilia-Romagna earthquake. *J. Geophys. Res. Solid Earth* **2017**, *122*, 5622–5638. [CrossRef]
2. Cubrinovski, M.; Rhodes, A.; Ntritsos, N.; Van Ballegooy, S. System response of liquefiable deposits. *Soil Dyn. Earthq. Eng.* **2018**, *124*, 212–229. [CrossRef]
3. Hurst, A.; Scott, A.; Vigorito, M. Physical characteristics of sand ejecta. *Earth-Sci. Rev.* **2011**, *106*, 215–246. [CrossRef]
4. Fontana, D.; Lugli, S.; Dori, S.M.; Caputo, R.; Stefani, M. Sedimentology and composition of sands ejected during the seismic crisis of May 2012 (Emilia, Italy): Clues for source layer identification and liquefaction regime. *Sediment. Geol.* **2015**, *325*, 158–167. [CrossRef]
5. Fontana, D.; Amoroso, S.; Minarelli, L.; Stefani, M. Sand Liquefaction Induced by a Blast Test: New Insights on Source Layer and Grain-Size Segregation Mechanisms (Late Quaternary, Emilia, Italy). *J. Sediment. Res.* **2019**, *89*, 13–27. [CrossRef]
6. Ishihara, K. Stability of natural deposits during earthquakes. In Proceedings of the Eleventh International Conference on Soil Mechanics and Foundation Engineering, San Francisco, CA, USA, 12–16 August 1985; pp. 321–376.

7. Bucci, M.G.; Villamor, P.; Almond, P.; Tuttle, M.; Stringer, M.; Ries, W.; Smith, C.; Hodge, M.; Watson, M. Associations between sediment architecture and liquefaction susceptibility in fluvial settings: The 2010–2011 Canterbury Earthquake Sequence, New Zealand. *Eng. Geol.* **2018**, *237*, 181–197. [CrossRef]
8. Amorosi, A.; Bruno, L.; Facciorusso, J.; Piccin, A.; Sammartino, I. Stratigraphic control on earthquake-induced liquefaction: A case study from the Central Po Plain (Italy). *Sediment. Geol.* **2016**, *345*, 42–53. [CrossRef]
9. Beyzaei, C.Z.; Bray, J.D.; van Ballegooy, S.; Cubrinovski, M.; Bastin, S. Depositional environment effects on observed liquefaction performance in silt swamps during the Canterbury earthquake sequence. *Soil Dyn. Earthq. Eng.* **2018**, *107*, 303–321. [CrossRef]
10. Bastin, S.H.; Ogden, M.; Wotherspoon, L.M.; Van Ballegooy, S.; Green, R.A.; Stringer, M. Geomorphological Influences on the Distribution of Liquefaction in the Wairau Plains, New Zealand, Following the 2016 Kaikōura Earthquake. *Bull. Seism. Soc. Am.* **2018**, *108*, 1683–1694. [CrossRef]
11. Bozzano, F.; Esposito, C.; Franchi, S.; Mazzanti, P.; Perissin, D.; Rocca, A.; Romano, E. Understanding the subsidence process of a quaternary plain by combining geological and hydrogeological modelling with satellite InSAR data: The Acque Albule Plain case study. *Remote Sens. Environ.* **2015**, *168*, 219–238. [CrossRef]
12. Thierry, P.; Prunier-Leparmentier, A.-M.; Lembezat, C.; Vanoudheusden, E.; Vernoux, J.-F. 3D geological modelling at urban scale and mapping of ground movement susceptibility from gypsum dissolution: The Paris example (France). *Eng. Geol.* **2009**, *105*, 51–64. [CrossRef]
13. Marache, A.; Breysse, D.; Piette, C.; Thierry, P. Geotechnical modeling at the city scale using statistical and geostatistical tools: The Pessac case (France). *Eng. Geol.* **2009**, *107*, 67–76. [CrossRef]
14. Touch, S.; Likitlersuang, S.; Pipatpongsa, T. 3D geological modelling and geotechnical characteristics of Phnom Penh subsoils in Cambodia. *Eng. Geol.* **2014**, *178*, 58–69. [CrossRef]
15. Calabrese, L.; Perini, L.; Lorito, S.; Luciani, P.; Martini, A.; Severi, P.; Correggiari, A.; Remia, A. 3D modelling of the Holocene succession in the southern Po Delta (Italy): From geology to applications. *Z. Dtsch. Ges. Geowiss.* **2016**, *167*, 339–352. [CrossRef]
16. Begg, J.G.; Jones, K.E.; Rattenbury, M.S.; Barrell, D.J.; Ramilo, R.; Beetham, D. A 3D geological model for Christchurch City (New Zealand): A contribution to the post-earthquake re-build. In *Engineering Geology for Society and Territory*; Springer: Cham, Switzerland, 2015; Volume 5, pp. 881–884.
17. Kruiver, P.P.; Wiersma, A.; Kloosterman, F.H.; de Lange, G.; Korff, M.; Stafleu, J.; Busschers, F.S.; Harting, R.; Gunnink, J.L.; Green, R.A.; et al. Characterisation of the Groningen subsurface for seismic hazard and risk modelling. *Neth. J. Geosci.* **2017**, *96*, s215–s233. [CrossRef]
18. Yazarlooa, R.; Khamehchiana, M.; Nikoodela, M.R. Observational-computational 3D Engineering Geological Model and Geotechnical Characteristics of Young Sediments of Golestan Province. In *Computational Research Progress in Applied Science & Engineering (CRPASE)*; PEARL Publication: Dhaka, Bangladesh, 2017; Volume 3.
19. Dhar, M.S.; Cramer, C.H. Probabilistic Seismic and Liquefaction Hazard Analysis of the Mississippi Embayment Incorporating Nonlinear Effects. *Seism. Res. Lett.* **2017**, *89*, 253–267. [CrossRef]
20. Boccaletti, M.; Bonini, M.; Corti, G.; Gasperini, P.; Martelli, L.; Piccardi, L.; Severi, P.; Vannucci, G. *Carta Sismotettonica della Regione Emilia-Romagna, Scala 1: 250.000. Note Illustrative. Regione Emilia-Romagna–SGSS, CNR-IGG*; SELCA Publisher: Florence, Italy, 2004.
21. Martelli, L.; Bonini, M.; Calabrese, L.; Corti, G.; Ercolessi, G.; Molinari, F.C.; Piccardi, L.; Pondrelli, S.; Sani, F.; Severi, P. *Carta Sismotettonica della Regione Emilia-Romagna e Aree Limitrofe. Note Illustrative. Regione Emilia-Romagna, Servizio Geologico, Sismico e dei Suoli*; D.R.E.A.M.: Pratovecchio, Italia, 2017.
22. *RER–ENI Riserve Idriche Sotterranee Della Regione Emilia-Romagna. G. M. Di Dio. Regione Emilia-Romagna, ENI Agip Divisione Esplorazione e Produzione*; SELCA Publisher: Florence, Italy, 1998; p. 120.
23. Basili, R.; Valensise, G.; Vannoli, P.; Burrato, P.; Fracassi, U.; Mariano, S.; Boschi, E. The Database of Individual Seismogenic Sources (DISS), version 3: Summarizing 20 years of research on Italy's earthquake geology. *Tectonophysics* **2008**, *453*, 20–43. [CrossRef]
24. Burrato, P.; Vannoli, P.; Fracassi, U.; Basili, R.; Valensise, G. Is blind faulting truly invisible? Tectonic-controlled drainage evolution in the epicentral area of the May 2012, Emilia-Romagna earthquake sequence (northern Italy). *Ann. Geophys.* **2012**, *55*, 525–531. [CrossRef]
25. Rovida, A.N.; Locati, M.; Camassi, R.D.; Lolli, B.; Gasperini, P. *CPTI15, the 2015 Version of the Parametric Catalogue of Italian Earthquakes*; Istituto Nazionale di Geofisica e Vulcanologia: Rome, Italy, 2016.
26. Castaldini, D. The Southern Central Sector of the Po Plain (Northern Italy): A geomorphological study with examples of evidence of paleorivers. *Jeomorfol. Derg.* **1990**, *18*, 1–10.
27. Emergeo Working Group. Liquefaction phenomena associated with the Emilia earthquake sequence of May–June 2012 (Northern Italy). *Nat. Hazards Earth Syst. Sci.* **2013**, *13*, 935–947. [CrossRef]
28. Papathanassiou, G.; Mantovani, A.; Tarabusi, G.; Rapti, D.; Caputo, R. Assessment of liquefaction potential for two liquefaction prone areas considering the May 20, 2012 Emilia (Italy) earthquake. *Eng. Geol.* **2015**, *189*, 1–16. [CrossRef]
29. Allen, R.L.J. *Sedimentary Structures, Their Character and Physical Basis*; Elsevier: Amsterdam, The Netherlands, 1982; Volume 1.
30. Marcaccio, M.; Martinelli, G. Effects on the groundwater levels of the May–June 2012 Emilia seismic sequence. *Ann. Geophys.* **2012**, *55*, 811–814. [CrossRef]

31. Pellegrini, M.; Zavatti, A. Il sistema acquifero sotterraneo tra i fiumi Enza, Panaro e Po: Alimentazione delle falde e scambi tra falde, correlazioni idrochimiche. *Quad. IRSA* **1980**, *51*, 206–217.
32. ARPAE. *La Qualità delle Acque Sotterranee in Provincia di Modena*; Report; ARPAE: Bologna, Italy, 2016.
33. Oliver, M.A.; Webster, R. Kriging: A method of interpolation for geographical information systems. *Int. J. Geogr. Inf. Syst.* **1990**, *4*, 313–332. [CrossRef]
34. Lai, C.G.; Poggi, V.; Famà, A.; Zuccolo, E.; Bozzoni, F.; Meisina, C.; Bonì, R.; Martelli, L.; Massa, M.; Mascandola, C.; et al. An inter-disciplinary and multi-scale approach to assess the spatial variability of ground motion for seismic microzonation: The case study of Cavezzo municipality in Northern Italy. *Eng. Geol.* **2020**, *274*, 105722. [CrossRef]
35. Robertson, P.K. Soil classification using the cone penetration test. *Can. Geotech. J.* **1990**, *27*, 151–158. [CrossRef]
36. Schmertmann, J.H. *Guidelines for Cone Penetration Test: Performance and Design. (No. FHWA-TS-78-209)*; Federal Highway Administration: Washington, DC, USA, 1978.
37. Meisina, C.; Persichillo, M.G.; Francesconi, M.; Creatini, M.; Uruci, E.; Lo Presti, D. Differences between mechanical and electrical cone penetration test in the liquefaction hazard assessment and soil profile reconstruction. In Proceedings of the ICCE International Conference of Civil Engineering, Tirana, Albania, 12–14 October 2017.
38. Jones, N.L.; Wright, S.G. Subsurface Characterization with Solid Models. *J. Geotech. Eng.* **1993**, *119*, 1823–1839. [CrossRef]
39. Lemon, A.M.; Jones, N.L. Building solid models from boreholes and user-defined cross-sections. *Comput. Geosci.* **2003**, *29*, 547–555. [CrossRef]
40. Working Group ICMS. Indirizzi e Criteri per la Microzonazione Sismica–Guidelines for Seismic Microzonation. Conferenza delle Regioni e delle Province Autonome-Dipartimento della Protezione Civile. 2008. Available online: https://www.protezionecivile.gov.it/it/pubblicazione/indirizzi-e-criteri-la-microzonazione-sismica (accessed on 28 March 2021).
41. Meisina, C.; Bonì, R.; Bordoni, M.; Lai, C.G.; Famà, A.; Bozzoni, F.; Cosentini, R.M.; Castaldini, D.; Fontana, D.; Lugli, S.; et al. 3D Geological model reconstruction for liquefaction hazard assessment in the Po Plain. In *Earthquake Geotechnical Engineering for Protection and Development of Environment and Constructions, Proceedings of the 7th International Conference on Earthquake Geotechnical Engineering, 7ICEGE, Istanbul, Turkey, 17–19 June 2013*; Silvestri, F., Moraci, N., Eds.; ITA: Rome, Italy, 2013; pp. 3837–3844.
42. Martínez, M.G.; Tonni, L.; Gottardi, G.; Rocchi, I. Analysis of CPTU data for the geotechnical characterization of intermediate sediments. In Proceedings of the 4th International Symposium on Cone Penetration Testing, Delft, The Netherlands, 21–22 June 2018; CRC Press: Boca Raton, FL, USA, 2018; pp. 281–287.
43. Silverman, B.W. *Density Estimation for Statistics and Data Analysis*; Chapman and Hall: New York, NY, USA, 1986.
44. Ninfo, A.; Zizioli, D.; Meisina, C.; Castaldini, D.; Zucca, F.; Luzi, L.; De Amicis, M. The survey and mapping of sand-boil landforms related to the Emilia 2012 earthquakes: Preliminary results. *Ann. Geophys.* **2012**, *55*, 727–733. [CrossRef]
45. Bignami, C.; Burrato, P.; Cannelli, V.; Chini, M.; Falcucci, E.; Ferretti, A.; Gori, S.; Kyriakopoulos, C.; Melini, D.; Moro, M.; et al. Coseismic deformation pattern of the Emilia 2012 seismic sequence imaged by Radarsat-1 interferometry. *Ann. Geophys.* **2012**, *55*, 789–795. [CrossRef]
46. Chini, M.; Albano, M.; Saroli, M.; Pulvirenti, L.; Moro, M.; Bignami, C.; Falcucci, E.; Gori, S.; Modoni, G.; Pierdicca, N.; et al. Coseismic liquefaction phenomenon analysis by COSMO-SkyMed: 2012 Emilia (Italy) earthquake. *Int. J. Appl. Earth Obs. Geoinf.* **2015**, *39*, 65–78. [CrossRef]
47. Nichols, R.J.; Sparks, R.S.J.; Wilson, C. Experimental studies of the fluidization of layered sediments and the formation of fluid escape structures. *Sedimentology* **1994**, *41*, 233–253. [CrossRef]
48. Youd, T.L.; Garris, C.T. Liquefaction-Induced Ground-Surface Disruption. *J. Geotech. Eng.* **1995**, *121*, 805–809. [CrossRef]
49. Lugli, S.; Marchetti, D.S.; Fontana, D. Alluvial sand composition as a tool to unravel the Late Quaternary sedimentation of the Modena Plain, northern Italy. In *Sedimentary Provenance and Petrogenesis: Perspectives from Petrography and Geochemistry: Geological Society of America Special Paper*; Arribas, J., Critelli, S., Johnsson, M.J., Eds.; Geological Society of America: Boulder, CO, USA, 2007; pp. 57–72.